A&A 426, 875–884 (2004)
DOI: 10.1051/0004-6361:20035929
© ESO 2004

Astronomy & Astrophysics

Coordinated observation of local interstellar helium in the Heliosphere

Modeling the interstellar-interplanetary helium 58.4 nm resonance glow: Towards a reconciliation with particle measurements

R. Lallement[1], J. C. Raymond[2], J. Vallerga[3], M. Lemoine[4], F. Dalaudier[1], and J. L. Bertaux[1]

[1] Service d'Aéronomie du CNRS, BP 3, 91371 Verrières-le-Buisson, France
e-mail: rosine.lallement@aerov.jussieu.fr
[2] Harvard Smithsonian Center for Astrophysics, 60 Garden Street, MS 50, Cambridge, MA 02138, USA
[3] Space Sciences Laboratory, University of California, Berkeley CA 94720-7450, USA
[4] Institut Leprince-Ringuet, École Polytechnique 91128 Palaiseau, France

Received 22 December 2003 / Accepted 14 May 2004

Abstract. Pioneering observations of the diffuse HeI-58.4 nm background radiation were performed with a series of satellites in the 70's. Today, their published results on the flow of interstellar helium atoms in the heliosphere are still in contradiction with (i) the results of the particle experiments, i.e. in situ detection of neutrals and pickup ions; (ii) expectations from heliospheric models and comparison with the hydrogen flow; (iii) results of the recent helium glow observations with the Extreme Ultraviolet Explorer (EUVE). Here we discuss these data sets and their modeling, together with the EUVE data and the first coronographic observations of the helium glow obtained with the Ultraviolet Coronographic Spectrometer (UVCS) on board SOHO. We show how they can all be made compatible, and reconciled with in situ data.

We have reanalysed the Prognoz data and we derive an updated and higher value of the background noise level. Based on this we can now fit the data satisfactorily with the same set of helium parameters as that one derived from recent EUVE and in situ data. We suggest that other early data sets could be reanalyzed in the same way.

Using this updated analysis, EUVE and SOHO-UVCS measurements, we find that all glow data are compatible with the interstellar parameters $V_0 \approx 25$ km s^{-1}, $T_0 \approx 6500$ K, $\lambda_0 \approx 74.0$ deg, $\beta_0 \approx 6.0$ deg (downwind axis, ecliptic coordinates), as well as with the solar parameters derived from SOHO CELIAS-SEM, SUMER and CDS observations, i.e. the helium photoionisation rate, the 58.4 nm irradiance, and the 58.4 nm Doppler width, found to be between 60 and 90 mÅ (30 and 45 km s^{-1}). The density is the least constrained parameter from the glow measurements. Prognoz lateral scans, EUVE LWS and SOHO UVCS data are compatible with an interstellar helium density n_0 in the range 0.013–0.016 cm^{-3}. Prognoz anti-solar data and EUVE scanner data lead to a 40% lower value, suggesting uncertainties in the calibrations. A large part of the contradictions between particle and remote sensing results are thus removed, since the above parameters are very similar to those derived from in situ data.

The high electron impact rates inferred from the UVCS remote sensing observations imply high fluxes of newly produced helium pickup ions, which can possibly explain in part the observed correlation between H^+ and He^+ pickup fluxes, and the inverse correlation between He^+ fluxes and solar wind velocity.

Key words. interplanetary medium – Sun: solar wind – plasmas – ISM: atoms – ISM: kinematics and dynamics

1. Introduction

Theoretical models predict a differentiation of interstellar neutrals at the heliospheric interface due to differential coupling with the plasma (Wallis 1975, 1984; Baranov & Malama 1993; Izmodenov et al. 1999). This phenomenon is helpful, because the comparison between the velocity distributions of the different species in the inner heliosphere provides an indirect measurement of the interstellar plasma density. In particular, neutral hydrogen is strongly coupled to the plasma by charge-exchange, and a slower and hotter population of charge-exchanged interstellar protons is created. At variance with H, helium is not coupled to plasma and is expected to remain unchanged. This invariance of helium is consistent with the excellent agreement between the Local Interstellar Cloud (LIC) properties (Lallement & Bertin 1992; Lallement et al. 1993; Linsky et al. 1993), and the helium temperature and velocity derived from direct in situ detection (Witte et al. 1993, 1996, 2004; Gloeckler et al. 2004).

Helium is thus a very useful tracer of the conditions prevailing in the ambient interstellar medium and is a point of reference for the other species. The amount of heating, deceleration and filtering of hydrogen, all three independent diagnostics of the interstellar plasma density are indeed measured by reference to helium (note that the filtration factor measurement is also dependent on the fractional ionization of helium in the LIC, found to be 35–40% from EUVE measurements of white dwarfs (Dupuis et al. 1995; Wolff et al. 1999).

Schematically there have been two periods of observations of HeI-58.4 nm radiation backscattered by streaming

Article published by EDP Sciences and available at http://www.aanda.org or http://dx.doi.org/10.1051/0004-6361:20035929

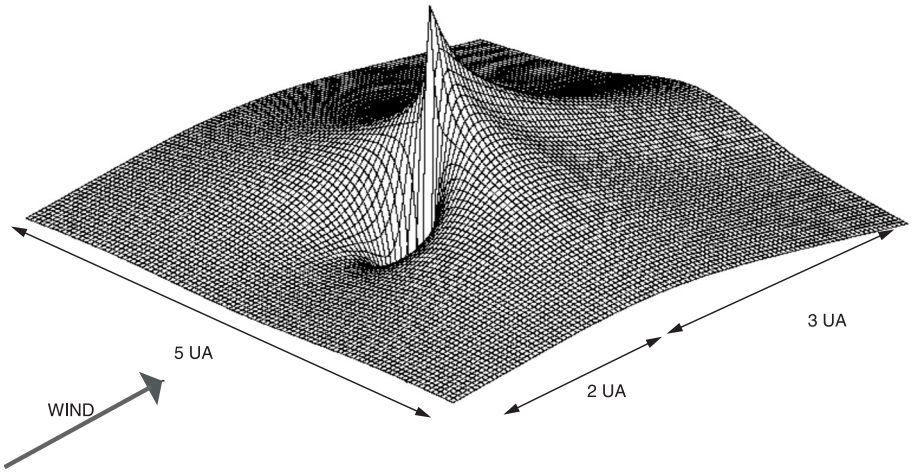

Fig. 1. Model helium 58.4 nm emissivity (logarithmic scale) for typical parameters. The secondary emission maxima at right angles with the wind (or equivalently the upwind minimum) are due to Doppler dimming effects and vary with the solar linewidth.

interstellar helium atoms (the so-called helium glow). A first series of data was recorded during the 70s on board STP-72, OSO-8, Solrad 11B, Mariner 10 and Prognoz5-6 by UV photometers (Weller & Meier 1974, 1979, 1981; Ajello 1978; Ajello et al. 1979; Dalaudier et al. 1984 (DBKM)). For a historical review, see Lallement (2002). The first pioneering measurements discovered the helium gravitational cone, but gave only broad ranges for the wind velocity, temperature and density. Models of the interstellar helium flow were adjusted to the more extended observations with Prognoz and Solrad 11, resulting in a helium temperature of ≈15–17 000 K (Weller & Meier 1981; Dalaudier et al. 1984), much higher than the hydrogen temperature derived at the same period from Prognoz 5 and 6 measurements, i.e. ≈8000 K (Bertaux et al. 1985). Since the models predict hydrogen heating and absence of change of the helium temperature, this was a puzzling result. Simultaneously, the helium velocity was found to be ≈27 km s^{-1}, above the Local Cloud velocity of ≈25.5 km s^{-1} (Lallement & Bertin 1992). It has to be recalled that the glow data obtained in the 70's and the 80's had in common the absence of any spectroscopic diagnostic (only the global emission pattern was used), and the absence of lines-of-sight (LOS) of less than 90 deg from the Sun direction. Later on, in situ sampling of interstellar helium atoms on board Ulysses (Witte et al. 1993, 1996) and charge/mass spectrometry of pickup helium ions (Möbius et al. 1985, 1995; Gloeckler et al. 1997, 2004; Noda et al. 2001; Oka et al. 2002), all favored a lower helium temperature. Indeed, these in situ data brought results in excellent agreement with the Local Cloud data ($V_0 \approx 25$ km s^{-1} and $T_0 \approx 6500$ K). Some new ideas were explored in a search for explanations of the discrepancies between the remote sensing results and the particle results, but no definitive and fully satisfying answer was found (Fahr et al. 1985; Chassefiere et al. 1988), casting some shadow on the glow data interpretation and the reliability of the interstellar plasma density determination from hydrogen heating and deceleration.

The second series of glow measurements has been made with the EUVE and SOHO-UVCS (Flynn et al. 1998, herafter FVDG; Michels et al. 2002), and it has brought entirely new perspectives. We describe in Sect. 3 their new characteristics, and more recent data and their analyses are described in detail in companion papers (Vallerga et al. 2004; Lallement et al. 2004). In these papers, as in the present one, it is also important to note that the solar 58.4 nm line intensity, its linewidth and its intensity temporal variations, as well as the helium photoionization rate ($\lambda \leq 50.4$ nm) and its solar cycle variations are now considerably more accurate, thanks to the CELIAS-SEM monitor and the UV spectrographs CDS and SUMER, all on-board SOHO (Wilhelm et al. 1997; Lemaire et al. 1997; Harrison et al. 1997; Judge et al. 2002; Lang et al. 2002; McMullin et al. 2004). These parameters have a direct impact on the helium density close to the Sun, and on the glow intensity.

In Sect. 2, we revisit the 1977 Prognoz data and present an inter-comparison of the Prognoz and EUVE measurements. We reanalyse the Prognoz data in the light of this comparison, and propose a solution to the long-standing discrepancies. We show new fits to the Prognoz data for parameters similar to the LIC or in situ parameters. In Sect. 3, we review all measurements, including the EUVE and UVCS data and compare with particle analyses. In Sect. 4, we discuss possible improvements of the modeling and the synergy between remote and in situ observations.

2. Prognoz data revisited

The model we use here is the classical kinetic model (the so-called hot model). Figure 1a shows the expected 58.4nm emissivity in a plane containing the Sun and the wind axis, for a standard set of parameters: $T = 7000$ K, $V = 25.5$ km s^{-1}, average solar conditions: solar linewidth (Doppler width or half-width at $\frac{1}{e}$) $W_D = 35$ km s^{-1}, photoionization rate $\beta = 1.0 \times 10^{-7}$ s^{-1}, and an isotropic Sun. For those parameters, the helium gravitational cone extends at large distances from the Sun, with a maximum density enhancement of ≃5 along the cone at 1.2 AU. At 45 AU the density is still enhanced by a factor of ≃2. The maximum emissivity region is within 0.1 AU from the Sun. The secondary maximum of emissivity at 90 deg from the wind direction is due to the influence of Doppler dimming effects. For a solar linewidth as narrow as $W_D = 35$–45 km s^{-1},

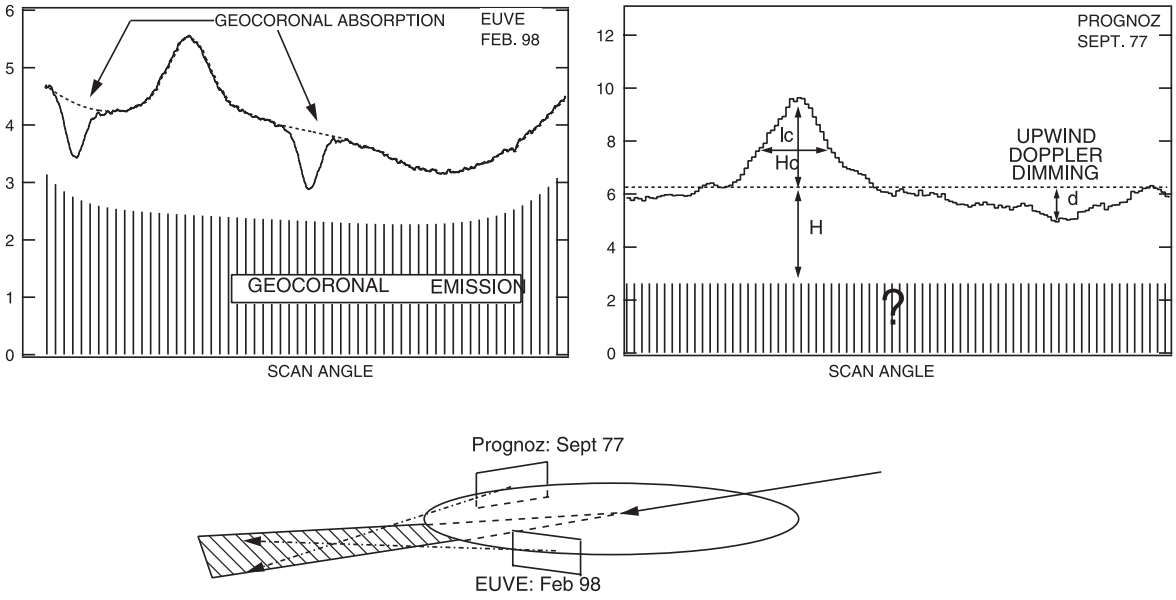

Fig. 2. Comparison between the Prognoz scan recorded in Sep. 1977 when the earth longitude was $\lambda_e = 5.5$ deg (*right*), and the EUVE scan recorded in Feb. 1998 ($\lambda_e = 147$ deg) (*left*). Within a few degrees these scans are symmetric with respect to the wind axis, and the solar activity cycle phase is the same. Intensity patterns should be similar (excepted for geocoronal absorption and emission in the case of EUVE). This suggests that background noise is contaminating the Prognoz data in the same way geocoronal emission contaminates EUVE data.

atoms located along the wind axis and flowing towards or away from the Sun at $V = 25$ km s^{-1} and more (due to gravitational acceleration) are significantly Doppler shifted out of the solar line center, i.e. they resonate with the wings of the line, which results in a significant decrease of the diffused intensity, the upwind (and downwind) Doppler Dimming. This effect disappears at right angles with the wind axis, producing the secondary maximum. The Doppler dimming amplitude (or the relative height of the secondary maximum) increases when the solar line width decreases.

Latitudinal anisotropies and temporal variations of the solar 58.4 nm intensity due to the irregular distribution of active regions on the solar surface and the solar rotation can significantly affect the pattern of the helium glow resonant emission. In most glow analyses, this must be taken into account in the modeling (see below). In the case of the Prognoz data, we have used the solar HeI 58.4 nm proxies based on the recent SOHO/SEM data (McMullin et al. 2004) to correct for the temporal variability. Prognoz measurements were done in 1976–1977, a period characterized by an exceptional amplitude of the variability, (fluctuations by a factor of 2), due to the presence of isolated active regions. One also expects the photoionisation, the electron impact and the irradiance to depend on the heliographic latitude (see McMullin et al. 2004), which removes the axisymetry of the density and emissivity distributions. This latitudinal variation is not included here in the case of the Prognoz data, but its effects are detected (see below).

The viewing geometry is about the same for the EUVE observations and the Prognoz 5-6 observations: two independent measurements are available in both cases: (i) scan planes perpendicular to the spin axis of the satellite, which is oriented along the Sun-Earth direction, and (ii) antisolar lines of sight. The main difference between the two experiments is the altitude of the satellite: the two Prognoz satellites had highly excentric orbits and data used for the analysis are those recorded at the apogee, i.e. at about 180 000 km. EUVE data were recorded at 500 km, i.e. within the exosphere, which implies that terrestrial helium scattering of the solar 58.4 nm light and absorption of the interplanetary diffuse emission by the geocorona are present. Another difference is, as we will see, the improved sensitivity of the detections (i.e. counts per Rayleigh) in the case of the more recent EUVE satellite.

Figure 2 shows the recorded 58.4 nm intensity in a scan plane such as the EUVE or Prognoz viewing planes (as shown at bottom). The cone intersection and the Doppler shift dimming on the upwind side are the main features. The relative amplitude of the cone intensity with respect to the average intensity (H_C vs. H) and the width of the cone l_C both depend on the ionization rate, the gas temperature and the solar line width. The upwind depression d, on the other hand, is anticorrelated with the ratio between the solar line width and the thermal width of the gas.

An important effect is that any error in the determination of the relative height of the cone emission H_C/H leads to coupled errors in the determination of the temperature, the ionization rate and the solar linewidth, all three simultaneously. This is why the determination of the "zero" level, or in other words of the background noise is crucial.

The data shown in Fig. 2 are EUVE and Prognoz intensities for scan planes exactly symmetric with respect to the wind axis, at an interval of two solar cycles, and for about the same phase of activity, in 1977 and 1998. It is interesting to compare carefully the two data sets. First, it is clear that Prognoz

data are much more irregular than EUVE data. Because the FOV's of the two instruments and the binning in angular cells are similar, the Prognoz irregularities probably do not reflect the 58.4 background. Comparing the solar indices for the two periods of time shows that the Prognoz period was characterized by stronger fluctuations of the solar 58.4 nm intensity (see below), but simulations of the effects of intensity variations as a function of longitude cannot produce the type of irregularities observed. They would induce smoother variations. In the past (before EUVE), those very large fluctuations of the recorded signal have been attributed to density inhomogeneities of the helium distribution, themselves due to temporal variations of the ionization. But irregularities are present also on the upwind side where ionization plays a smaller role and, again, such ionization variations produce much smoother effects. In the light of the new EUVE data, it appears now that these features are very likely the consequence of another phenomenon, specific to Prognoz, very probably instrumental noise. Now, if instrumental noise produces fluctuations in the signal of the order of 1 Rayleigh, it unfortunately raises questions about the average level of this noise, and its possibly large value in comparison with the true signal.

Second, it is immediately noticeable that the relative amplitude of the focusing cone enhancement in the Prognoz scan is similar to the one of the EUVE cone. This should not be the case, because the EUVE signal is the sum of the background emission, plus a strong geocoronal emission, see Flynn et al. (1998). This suggests that the Prognoz signal, as the EUVE signal, contains an extra component. It cannot be geocorona, because data have been recorded far enough from the Earth, thus it again speaks in favor of strong background noise, much stronger than previously estimated, and presumably solar wind particle effects. The method used for the Prognoz 58.4 nm background determination is detailed by DBKM. Briefly, they used the 30.4 nm channel as a particle detector. The 30.4 nm channel is located parallel to the 58.4 nm channel, and built in a similar way except for the entrance windows and filters. Its low sensitivity and the weakness of the 30.4 nm background resulted in a negligible photon-produced signal. Solar wind particle events produce strongly correlated counting peaks in both channels. According to the chosen correction procedure, 58.4 nm data were rejected each time the 30.4 nm channel signal rose above a given threshold. Otherwise, data were assumed to be uncontaminated (except for dark current noise measured prior to launch). For more details, see p. 173 and Fig. 4 of DBKM. We analyze this figure in a different way and estimate that the average count level of ≈2 units in the 30.4 nm channel (outside the events) is also largely due to background solar wind particles, and not to electronic dark current only, as somewhat arbitrarily assumed. Using the sensitivity ratio (deduced from strong solar wind events seen in both channels) this permanent noise in the 30.4 nm channel corresponds to a few counting units (1–2 Rayleigh) of background particle noise in the 58.4 nm channel.

The existence of such a strong background could explain the similarity of the general aspect of the EUVE and Prognoz scans (except for regularity), the background noise and the geocoronal signal playing about the same role and being by chance of about the same order. For Prognoz, the assumption of a higher level of noise immediately relaxes one of the strongest constraints on the modeling, i.e. the small upwind dimming (see Fig. 2). In the initial analysis with an assumed low background level, the relative depth of the upwind depression d was found to be small enough to preclude solar lines narrower than 55–60 km s^{-1} Doppler width. But this in turn had consequences for the focusing cone fitting, because the Doppler dimming is about the same in the downwind region and reduces the cone emission. A wide solar line implies a brighter cone (and a larger H_C/H). In order to balance this cone brightness, a high ionization rate is required (DBKM found 1.25×10^{-7} s^{-1}), which decreases the relative brightness but simultaneously reduces the *FWHM* of the cone. Finally, in order to balance this narrow *FWHM* the helium temperature is increased, which explains the 16 000 K found by DBKM.

The three parameters, temperature, linewidth, ionization rate are strongly linked for a given scan pattern. Allowing a higher background noise relaxes the constraint on dimming and in turn on the linewidth, and subsequently allows fits to the data with a lower temperature and a lower ionization rate, as shown in Fig. 3. It is interesting to see that those parameters, which were all three contradicted by the new solar and interstellar data, are now in much better agreement with (i) the linewidth measured by SUMER and CDS, i.e. 35–45 km s^{-1} Doppler width, (2) the ionization rate estimated from SOHO-SEM to be $\approx 0.6 \times 10^{-7}$ s^{-1}, and (iii) the temperature deduced from particle data (Witte et al. 2004; Gloeckler et al. 2004).

Figure 3 shows three typical Prognoz-6 scans, and compares the fits obtained by Dalaudier et al. (1984) and those obtained for a set of parameters close to the best-fit values of EUVE and GAS, as well as the required background for such fits. The background noise level is about 4 times the level assumed by DBKM. The quality of the fits is about the same, in both cases.

Searches for best fits to all lateral and antisolar Prognoz data have been done, allowing now, at variance with the previous analyses, for a freely varying background level for each individual scan. This background is assumed to be constant during the two or three days' duration of a scan. The solar flux used in the model is based on the 58.4 proxy discussed in McMullin et al. (2004) and uses the classical corotation calculation, i.e. it is assumed that the solar pattern is kept constant at the sun surface during up to half a solar rotation. During the line-of-sight integration, the disk-integrated flux is calculated for each individual location. The velocity vector has been kept fixed and assumed to be the one measured by Ulysses/GAS, ULYSSES/SWICS and the EUVE, but ionisation rate, temperature and linewidth were allowed to vary. Data-model adjustments lead to the following results: the minimum chi-square is now found for a temperature of about 10 000 K, an ionisation rate of 0.8×10^{-7} s^{-1} and a 40–45 km s^{-1} Doppler width, but the allowed range of parameters contains a number of combinations of β, W_D and T including T = 7000 K, $\beta = 0.6 \times 10^{-7}$ s^{-1} and W_D = 35–40 km s^{-1} (Doppler width). This is demonstrated by Fig. 4, which shows the entire data set (15 lateral and 15 anti-solar scans), with the favoured parameter set model superimposed on the data. It is clear that both models

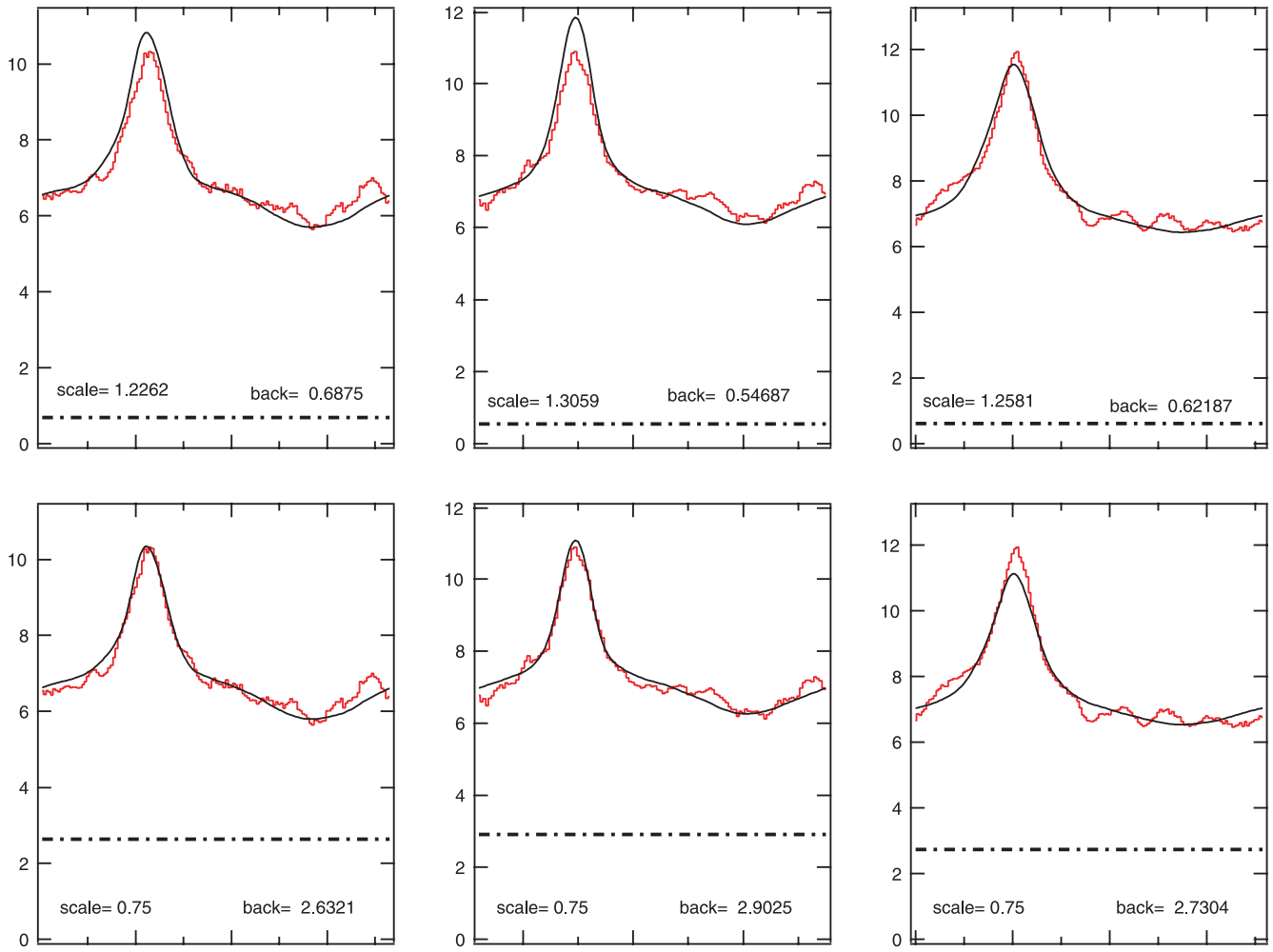

Fig. 3. A reanalysis of Prognoz data: comparison between best-fit models assuming the Dalaudier et al. (1984) background noise (*top*), and the best-fit model assuming different sensitivities and background levels (*bottom*). The model parameters are $V_0 = 27$ km s^{-1}, $T_0 = 16\,000$ K, $\beta = 1.25 \times 10^{-7}$ s^{-1}, and $V_0 = 25$ km s^{-1}, $T_0 = 7000$ K, $\beta = 0.8 \times 10^{-7}$ s^{-1} respectively.

are equally acceptable. The differences are fully compensated by background level variations.

As a consequence, we are convinced that Prognoz measurements can no longer be considered incompatible with other data sets. On the contrary, they reinforce the conclusions which are drawn from the EUVE analysis and the resulting set of parameters. For a solar line of 35 km s^{-1} (which implies a background value of $\simeq$2 counts instead of the initial value of 0.6 counts), the cone shape is well represented by the combination of $T = 7000$ K and $\beta = 0.8 \times 10^{-7}$ s^{-1}. It is interesting to note that the residuals show a small, but definitely present correlation with the ecliptic latitude. The trend can be interpreted as increased background noise, or higher illuminating flux at low latitude, or a combination of the two effects. Latitudinal anisotropies of the solar flux and of the ionization can certainly be present, and we will come back to this point in Sect. 4.

Using the calibration of Dalaudier et al. (1984) and the scaling factor obtained for the best fit to the lateral scan data with a variable background noise, we obtain for the He 58.4 proxies and the model of Fig. 4 a density of 0.0145 ± 0.003 cm^{-3}. However, the density derived from the antisolar channel is significantly smaller (by about 40%), which illustrates the difficulties in obtaining accurate calibrations for diffuse sources.

3. The series of glow data, their specific advantages, and derived parameters

Thanks to differences between instruments and observing conditions, each experiment that observed the diffuse He-I 58.4 nm background has brought its own original contribution. We discuss here this complementarity and which independent determinations of helium flow or solar parameters they allow. Then using these numbers we discuss the values of the interdependent parameters.

The STP-72 rocket experiment (Weller & Meier 1974, 1981) was the pioneering observation, where most of the features of the glow were observed. The focusing cone, direction of the flow, and measurements of the magnitude of the signal helped to design the new experiments. However, the ranges of velocity and temperature derived from data modeling are very broad, due to the limited data set. Subsequent measurements with OSO-8, Solrad 11-B, and Mariner 10 confirmed the

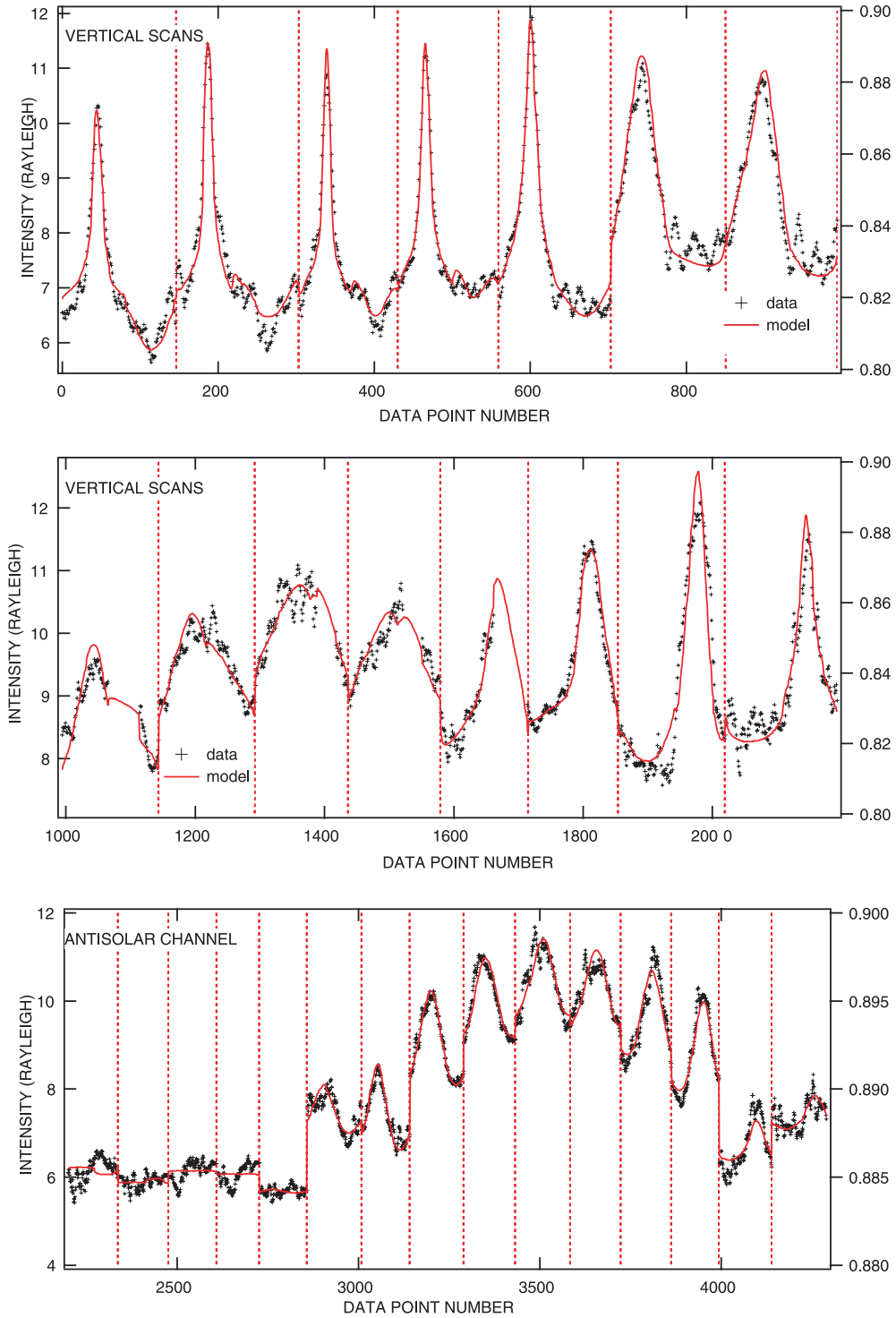

Fig. 4. Prognoz data: fits to the 30 scans (15 vertical planes and 15 scans around the anti-sun direction), see Dalaudier et al. 1984 for data description. The model parameters are 7000 K, $V_0 = 25.4$ km s^{-1}, $W_D = 40.0$ km s^{-1}, $\lambda_0 = 74.5$ deg, $\beta_0 = -6.0$ deg. Intensities are corrected for solar flux variations at each point along the LOS according to the 58.4 nm proxy (McMullin et al. 2004). A constant background noise is adjusted separately for each scan.

general features of the glow, and narrowed the parameter ranges, but again the sky coverage and the number of vantage points were limited, leaving room for a large number of parameter sets. In general, the model parameters, velocity, temperature and direction for all these experiments are in good agreement with the parameters subsequently derived by Dalaudier et al. (1984) from the Prognoz-5 and 6 photometers. This is why we have, in the previous section, focused on the reanalysis of the latter data, which cover a larger range of directions of sight and earth locations. We have shown how

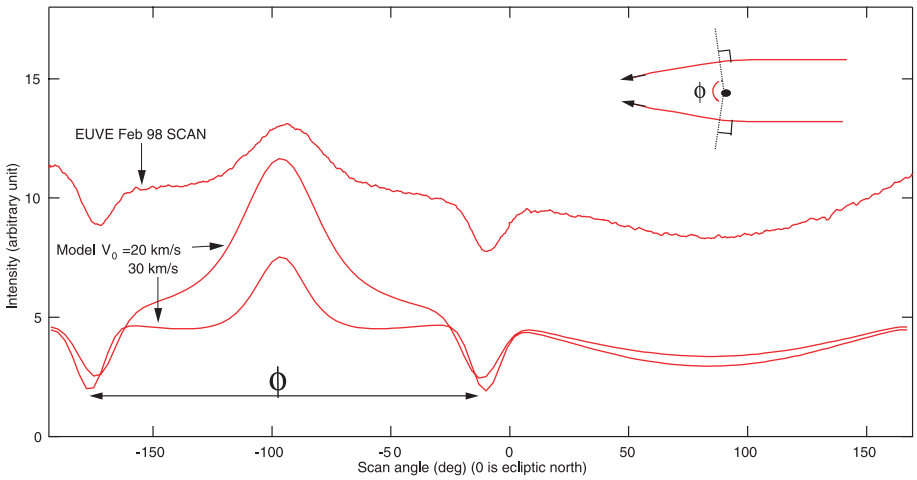

Fig. 5. Influence of the velocity modulus on the direction of the geocoronal absorption features: example of the EUVE Feb. 98 scan. Note that the data have been arbitrarily offset, and that they contain the geocoronal emission.

sensitive the model results are to noise estimates and also to assumptions about solar parameters. We think that this is applicable to earlier data sets other than Prognoz, and that they cannot be considered as incompatible with the parameter range deduced from new particle and EUVE glow measurements.

The main advantage of Prognoz-type data is the total absence of geocoronal contamination. This makes it possible to get the shape of the intensity pattern, although as we have seen a background noise is likely to be present at a significant level. This is very precious when analyzing data obtained from lower altitudes. It is for example clear from Fig. 2 that the emission enhancements recorded by the EUVE Scanner at high zenith angles on the left and right parts of the scan in the figure are not interstellar helium emission, since they are not seen with Prognoz for the same geometry. Therefore they are attributed to terrestrial helium.

One particularity of helium glow modeling, when it is based only on intensity measurements in vertical planes, is that, except for the flow direction, other parameters cannot be derived independently, as illustrated in Sect. 2. This is why the EUVE data (see Vallerga et al. 2004) have two strong advantages above other data sets: (i) a unique set of uncontaminated anti-solar data recorded from a full earth orbit around the sun; (ii) the existence of the geocoronal absorption features. In addition, the data are characterized by a high signal to noise ratio (see Fig. 3).

The EUVE anti-sun data, with line-of-sight entirely in the earth shadow and thus no geocoronal emission, provide the best and quasi-independent measurement of the solar line width, thanks to the upwind Doppler dimming. The value derived is also confirmed by the lateral scans, provided other parameters are given their appropriate values. The internal contradiction contained in the FVDG results, i.e. a Doppler width $\Delta w_{\rm D} = 30$ km s^{-1} for the anti-sun data and $\Delta w_{\rm D} = 60$ km s^{-1} for the scanner data, is now removed in Vallerga et al. (2004).

The anti-sun data also provide a precise measurement of the flow longitude, with an accuracy of less than 0.5 degree after solar brightness fluctuations have been carefully removed. In the first analysis, FVDG found a wind longitude shifted by 2 degrees from the direction deduced from particle data and Prognoz data. In the new analysis (Vallerga et al. 2004) this discrepancy is resolved and the agreement is now excellent.

The geocoronal absorption features on the other hand provide spectroscopic information, because their locations depend on the vectorial difference between the helium flow velocity vector and the earth motion. Figure 5 shows the EUVE Feb98 scan data and model results for three different values of the bulk velocity of the helium flow, as a function of the azimuthal angle in the scan plane. The larger the helium flow velocity, the less the bending of the helium trajectories under the action of gravitational forces due to inertia, and the lower the deviation of the flow close to the Sun. The geocorona, acting as an absorption cell, produces maximum absorption when the line-of-sight (LOS) projected Doppler velocity of helium is zero in the earth frame, i.e. when the LOS is perpendicular to the relative flow vector. For the vertical scan planes this happens at high ecliptic latitude, i.e. for very small values of the LOS projected earth velocity vector (see Fig. 5). In the limit of very high flow velocities, inertial forces are such that the bulk velocity remains the same everywhere, and maximum absorptions occur in the two opposite directions perpendicular to the initial bulk flow vector. When there is focusing, the angle between the two directions of maximum absorption (angle ϕ of Fig. 5) is smaller, and its measurement is an independent measurement of the velocity V_0. The temperature is thus unambiguously determined, which explains why the FVDG results, namely a velocity of $\simeq$26 km s^{-1} and a temperature of $\simeq$7000 K, were the first results compatible with in situ data analyses. This method is again used in the EUVE companion paper to derive V_0. In vertical planes however, an additional and relatively small convergence of the flow is induced by the latitudinal anisotropy of the ionization, which is not accounted for in the modelling, and will be the subject of forthcoming studies. We expect a small systematic error of the order of 1 km s^{-1} linked to this anisotropy.

As can be seen in Fig. 5 V_0 influences the angle $\Delta(\theta)$ between the two absorption features. At variance with V_0, the influence of the flow latitude β_0 on $\Delta(\theta)$ is, for obvious geometrical reasons, null, and changing β_0 by an increment $\delta(\beta_0)$ results

simply in a shift of both absorptions by an angle $\delta(\beta_0)$. This interestingly decouples the determinations of V_0 and β_0. For the determination of β_0 from the absorption features in the lateral scans very accurate knowledge is required of the direction of the LOS, and e.g. to take into account very carefully any small offset between the LOS of the different channels, as discussed in Vallerga et al. In principle however, such a measurement can be extremely precise.

Numerical results from the EUVE analysis and other glow data are the following (independently determined parameters only): $\lambda_0 = 74.7 \pm 0.5°$, $\beta_0 = -5 \pm 1°$, $V_0 = 24.5 \pm 2$ km s^{-1}, $w_D = 35 \pm 5$ km s^{-1} (Doppler width). The three flow vector parameters are found to be compatible with those derived from particle data. As already discussed, the rather low value of V_0 is very likely due to anisotropic ionisation and will be the subject of forthcoming studies. The fourth (solar) parameter is in agreement with the recent spectroscopic measurements by CDS and SUMER on board SOHO. The two spectrographs have observed a number of regions on the disk, and although there is a significant variability, the average value is constant with the activity and found to be around 35 km s^{-1} (McMullin et al. 2004). In the case of SUMER there have been additional off-disk spectral measurements using the scattered light, a method suggested by J.L. Bertaux in 1995, which have the advantage of providing the disk-integrated linewidth (see Lemaire et al. 1998). The measurements in 1996 and 2002 give $W_D = 81 \pm 6$ mÅ (41 ± 3 km s^{-1}) and 75 ± 6 mÅ (38 ± 3 km s^{-1}), respectively (Lemaire 2003). It is interesting to see that there is a good convergence between the direct measurement and the result of glow data modeling.

The UVCS observations are the first measurements of the interstellar helium diffuse emission with an EUV solar coronograph. For a solar angle of 1.75°, or 7 Rs (Rs = solar radius), the corresponding L-O-S cross the helium cone at about 0.20 and 0.33 AU from the Sun in December and June respectively (Fig. 4 from Lallement et al. 2004), much closer to the Sun than any other 58.4 experiment, and in its region of maximum emissivity. This is why, although UVCS intensities cannot be used to derive the flow parameters, they bring unique information on the ionization processes. A strong intensity decrease (by more than 10) from solar minimum to maximum activity has been measured. Such a decrease cannot be explained by a photoionization increase alone, and requires another mechanism. Assuming proxy values for the photoionization rate and the solar line, and an interstellar density of 0.015 cm^{-3} (from in situ data), the UVCS analysis infers a strong increase with the solar activity of this additional ionization, likely to be mostly electron impact ionization, with a possible contribution of double charge-exchange with solar wind alphas (see Lallement et al. 2004). The importance of solar wind electron impact on neutral helium within 1 AU has been predicted by Holzer (1977) and rates have been calculated by Rucinski & Fahr (1989), Fahr (1990), and Rucinski et al. (1993, 1996). The UVCS data imply ionization rates on the high side of the estimated range. It is interesting to note that the inferred increase by a factor of 3.5 of the electron impact rate between 1996 and 2001 follows closely the increase by about the same factor of the coronal electron density between 2 and 5 R_S measured by the white light coronograph (LASCO) on board SOHO (Lamy et al. 2002).

The electron impact ionization does not influence significantly the helium density beyond 1 AU, i.e. most data from EUVE or Prognoz can be fitted without including it, except for LOS along the cone, as in the antisolar data. Electron impact ionization has been included in the EUVE data analysis, at a rate estimated from the UVCS analysis and adapted to the solar activity phase.

In what follows we adopt the parameters which are determined independently, and we discuss the constraints on the remaining parameters. The remaining interstellar parameters are the temperature T_0 and the density n_0, and the remaining solar parameters are the photoionization rate β_{ph}, the electron impact ionization rate, and the solar 58.4 nm line intensity F_S. With photo-ionization taken from the proxies and e-impact ionization chosen according to the activity and the UVCS results, it is possible to derive the interstellar flow temperature from the cone brightness and shape. In the case of the EUVE (LWS) anti-sun data, a temperature of 7000 K is found to fit the observed focusing cone. In the case of vertical scans, both Prognoz and EUVE, the cone appears to be broader, i.e. the derived temperature is higher than 7000 K, and contained within the 8000–10 000 K range. We derive from these differences that ionization anisotropies probably play a role, i.e. the density in the central part of the cone at low ecliptic latitude is lower than predicted by the isotropic model, due to a stronger ionization close to the ecliptic, which for a vertical scan mimics a broader cone and a higher temperature. However, the decrease of the solar irradiance with heliolatitude has a somewhat opposite effect, and further studies based on more sophisticated solar models (see McMullin et al. 2004) are required to disentangle these two factors. There may also be some non-stationarity effects, which tend to defocus the cone and mimic a higher temperature.

Density is probably the least precisely determined parameter, for a number of reasons. The main one is the well known difficulty of obtaining an accurate value of the sensitivity to diffuse sources of the various instruments. A second one is the strong dependence of the emissivity on the solar ionization, which is highly time-variable. Then there is the solar irradiance directional and time variability. In particular latitudinal anisotropies, which have been neglected in most studies, are not negligible (see McMullin et al. 2004), and are indeed revealed in the Prognoz reanalysis of Sect. 2, as well as in the temperature and velocity modulus determination with the EUVE vertical scans. A density of 0.0135 ± 0.003 cm^{-3} is derived from the EUVE LWS data, assuming the instrument calibration is precisely known. In the same way, using the calibration of Dalaudier et al. (1984) and the proxies for 1977, we derive from Prognoz data fitting with a variable background a density of 0.0145 ± 0.003 cm^{-3}. Finally, the UVCS measured intensities are compatible with $n_0 = 0.015$ cm^{-3}, assuming irradiance and photoionization from proxies. In contradiction with these three determinations, which are in rather good agreement, the EUVE Scanner data (vertical scans), analyzed with the same model and for the same solar parameters as the antisolar data, lead to a lower density of the order of 0.08 cm^{-3}.

In the case of Prognoz, the situation is reversed. It is the antisolar channel which, again with the same model as the one used for the vertical scans, leads to a lower density of $\simeq 0.09$ cm^{-3}.

4. The synergy between remote sensing and in situ observations

The compatibility between the parameter ranges derived from remote sensing and in situ data gives better confidence in the models, and somehow increases the accuracy of these parameters. This duality may also have interesting consequences. An example is the electron impact ionization rate derived from the UVCS coronographic observations. When extrapolating the strong impact rates derived from these data within 0.2–0.3 AU, and assuming the radial dependence of Rucinski et al. (1996, 1998), the resulting fluxes of He^+ pickup ions (PUIs) generated after electron impact appear very high. At solar maximum and at 1 AU these ions represent within the above assumptions up to 34% of the total number of pickup ions (and 25% at solar minimum, Lallement et al. 2004). This fraction however is an average over time periods longer than a month, during which the solar wind fluctuates with large amplitudes. Increases or decreases of its flux and of its suprathermal electron content must be followed by large amplitude variations of the fluxes of generated pickup ions. In strong solar wind enhancements, it may happen that the majority of the produced ions is due to electron impact. This may play a role in the two very surprising correlations which have been discovered with the new generation of plasma spectrometers. The first correlation is between the He^+ PUI's flux and the pickup proton flux (Gloeckler et al. 1994), and the second is between the He^+ PUI flux and the inverse of the solar wind bulk velocity (Litvinenko et al. 1998). Because pickup protons are formed after charge-exchange between interstellar hydrogen and solar wind protons, any increase of the solar wind flux is followed by an increase of the pickup H^+ flux. At variance with H, He^+ pickup ions are essentially formed after photoionization, therefore one does not expect any link between the two pickup species. The correlation can have its source in transport effects (see Gloeckler et al. 1994) but there may be an additional role of e-impact. As a matter of fact, if in solar wind enhancements electron impact becomes the major source of He^+, both He^+ and H^+ are linked to the solar wind, and then in these enhancements a correlation between He^+ and H^+ can be established.

Explanations for the anti-correlation of He^+ fluxes with the solar wind velocity have remained elusive. Isenberg & Lee (1999) analyzed the effect of differential pitch-angle scattering, and concluded it could not play a role in the correlation. The e-impact production could have a role if one considers the following three reasons. First, it is well known that the slow wind is characterized by higher fluxes, compared to the high speed wind (e.g. Lallement et al. 1985; Goldstein et al. 1996). Second, and more important, density enhancements in the slow wind are much more frequent and much stronger than in the high speed wind. And third, suprathermal electron tails, which can efficiently generate PUIs, are more often encountered in the slow wind. Alltogether this may explain part of the observed higher variability and higher fluxes of He^+ PUI's in the slow wind. If confirmed, these results illustrate the complementarity between remote sensing and direct measurements.

5. Conclusions: Helium parameters and comparison with Hydrogen

The combination of helium glow data from different time periods, with different instruments, and in very different observing conditions, have brought better constraints on both the helium distribution and the solar parameters governing this density distribution, and the backscattered emission. In parallel, model improvements have resulted in a better understanding of the physical processes. The longstanding discrepancy between the UV-derived (from the first generation of instruments) and particle-derived parameters has been understood, thanks to the high signal to noise data of the EUVE, the comparison between EUVE and Prognoz data for the same observing geometry and solar conditions, and the possibility to use the geocorona as an additional spectrometric tool. The ionization processes close to the Sun have been measured for the first time with the SOHO/UVCS, providing new insights in the electron impact ionization evolution with solar activity and in the resulting PUI fluxes generated in the inner heliosphere.

The helium flow velocity vector, temperature and density correspond to the unperturbed state of the interstellar gas in the Local Interstellar Cloud (LIC), and hydrogen properties can now be analyzed in this reference frame. The temperature and velocity differences between hydrogen and helium are due to charge-exchange with the ionized interstellar gas at the periphery of the heliosphere. In the past, a first estimate of the hydrogen deceleration at entrance in the heliosphere has been derived from Ly-alpha Hubble Space Telescope spectra and Prognoz backscatter data on the one hand, and Ulysses results on helium and astronomical data on the other. A deceleration of $\simeq$5–6 km s^{-1} has been found (Lallement et al. 1993). According to models such a deceleration corresponds to an interstellar plasma density $n_e \approx 0.05$–0.10 cm^{-3}.

This determination can be greatly improved thanks to the new and more precise results on the helium flow discussed in this series of papers, and thanks to the interstellar hydrogen glow data continuously gathered by the SWAN experiment on board SOHO, which make it possible to establish an extensive data base for the hydrogen density distribution. A fraction of the SOHO/SWAN hydrogen cell data has been analyzed in two independent ways by Quemerais et al. (1999), and Costa et al. (1999). The two methods agree on the average velocity and temperature of the neutral hydrogen flow before its interaction with the supersonic solar wind within 50 AU, found to be $T(\mathrm{H}) = 11\,000$ K–$12\,000$ K, $V(\mathrm{H}) = 21$–22 km s^{-1}. After comparison with the helium velocity and temperature, the inferred heating and deceleration of about 4000 K and 4 km s^{-1} of the hydrogen flow has been preliminarily interpreted by Lallement (1999) and Izmodenov et al. (1999) as due to the effect of the theoretical heliospheric interface formed if the interstellar plasma density of the order of 0.04 cm^{-3}. Better constraints are expected from the combination of the present EUV results, present and future results from particle measurements, and future SOHO/SWAN data analyses.

Acknowledgements. This work has been carried out with support from the International Space Science Institute (ISSI) in Bern Switzerland. R.L., J.R., and J.V. are indebted to ISSI for the stimulating atmosphere and the great hospitality.

References

Ajello, J. M. 1978, ApJ, 222, 1068
Ajello, J. M., Witt, N., & Blum, P. W. 1979, A&A, 73, 260
Baranov, V. B., & Malama, Y. G. 1993, J. Geophys. Res., 98, A9, 15157
Bertin, P., Lallement, R., Ferlet, R., & Vidal-Madjar, A. 1993, J. Geophys. Res., 98, 15193
Chassefiere, E., Dalaudier, F., & Bertaux, J. L. 1988, A&A, 201, 113
Costa, J., Lallement, R., Quémerais, E., et al. 1999, A&A, 349, 660
Dalaudier, F., Bertaux, J. L., Kurt, V. G., & Mironova, E. N. 1984, A&A, 134, 171
Dupuis, J., Vennes, S., Bowyer, S., Pradhan, A. K., & Thejll, P. 1995, ApJ, 455, 574
Fahr, H. J., Nass, H. U., & Rucinski, D. 1985, A&A, 142, 476
Fahr, H. J. 1990, in Physics of the Outer Heliosphere, ed. Grzedzielski, et al. (Pergamon), 327
Flynn, B., Vallerga, J., Dalaudier, F., & Gladstone, G. R. 1998, J. Geophys. Res., 103, 6483, (FVDG)
Gloeckler, G., Jokipii, J. R., Giacalone, J., & Geiss, J. 1994, Geoph. Res. Lett., 21, 1565
Gloeckler, G., & Geiss, J. 2004, Adv. Space Res., in press
Gloeckler, G., Möbius, E., Geiss, J., et al. 2004, A&A, 426, 845
Goldstein, B. E., Neugebauer, M., Phillips, J. L., et al. 1996, A&A, 316, 296
Harrison, R. A., Fludra, A., Pike, C. D., et al. 1997, Sol. Phys., 170, 123
Holzer, T. E. 1977, Rev. Geophys. Space Phys., 15, 467
Isenberg, P. A., & Lee, M., Solar Wind Nine, ed. Habbal, et al., AIP 471, 815
Izmodenov, V. V., Geiss, J., Lallement, R., et al. 1999, J. Geophys. Res., 104, 4731
Judge, D. L., Ogawa, H. S., McMullin, D. R., Gangopadhyay, P., & Pap, J. M. 2002, Adv. Space Res., 29, 1963
Lallement, R., Bertaux, J. L., & Kurt, V. G. 1985, J. Geophys. Res., 90, 1413
Lallement, R., & Bertin, P. 1992, A&A, 266, 479
Lallement, R. 1993, Adv. Space Res., 13, 113
Lallement, R., Bertaux, J., & Clarke, J. T. 1993, Science, 260, 1095
Lallement, R. 1999, Solar Wind Nine, ed. S. R. Habbal, R. Esser, J. V. Hollweg, & P. A. Isenberg AIP 471, 205
Lallement, R. 2002, in The Century in Space, ed. Bleeker, Geiss, Huber (Kluwer Ac. Publ.)
Lallement, R., Raymond, J., Bertaux, J. L., et al. 2004, A&A, 426, 867
Lamy, P., Llebaria, A., & Quemerais, E. 2002, Adv. Space Res., 29, 373
Lemaire, P., Wilhelm, K., Curdt, W., et al. 1997, Sol. Phys., 170, 105
Lemaire, P., Emerich, C., Curdt, W., Schuehle, U., & Wilhelm, K. 1998, A&A, 334, 1095
Linsky, J. L., Brown, A., Gayley, K., et al. 1993, ApJ, 402, 694
Lang, J., Thompson, W. T., Pike, C. D., Kent, B. J., & Foley, C. R. 2002, in The radiometric calibration of SOHO, ISSI Scientific Report, ed. A. Pauluhn, M. Huber, & R. Von Steiger
Lemaire, P. 2003, private communication
Litvinenko, Y., Möbius, E., Grunwaldt, H., et al. 1998, EOS Trans. AGU, 79, 17, Spring Meeting Suppl., S269
McMullin, D. R., Judge, D. L., Phillips, E., et al. 2002, From Solar Min to Max, ESA SP-508, 489
McMullin, D. R., Bzowski, M., Möbius, E., et al. 2004, A&A, 426, 885
Michels, J. G., Raymond, J. C. , Bertaux, J. L., et al. 2002, ApJ, 568, 385
Möbius, E., Rucinski, D., Isenberg, P. A., et al. 1995, Adv. Space Res., 16, 357
Möbius, E. 2004, Adv. Space Res., in press
Möbius, E., Bzowski, M., Chalov, S., et al. 2004, A&A, 426, 897
Noda, H., Terasawa, T., Saito, Y., et al. 2001, Space Sci. Rev., 97, 423
Oka, M., Terasawa, T., Noda, H., Saito, Y., & Mukai, T. 2002, Geophys. Res. Lett., 29, 54
Quémerais, E., Bertaux, J., Lallement, R., et al. 1999, J. Geophys. Res., 104, 12585
Rucinski, D., & Fahr, H. J. 1989, A&A, 224, 290
Rucinski, R., Fahr, H. J., & Grzedzielski, S. 1993, Plan. Space Sci., 41 (10), 773
Rucinski, R., Cummings, A. C., Gloeckler, G., et al. 1996, Space Sci. Rev., 41, 773
Vallerga, J. 1996, Space Sci. Rev., 78, 277
Vallerga, J., Lallement, R., Raymond, J., et al. 2004, A&A, 426, 855
Weller, C. S., & Meier, R. R. 1981, ApJ, 246, 386
Wallis, M. K. 1975, Nature, 254, 202
Wallis, M. K. 1984, A&A, 130, 200
Weller, C. S., & Meier, R. R. 1974, ApJ, 193, 471
Weller, C. S., & Meier, R. R. 1979, ApJ, 227, 816
Weller, C. S., & Meier, R. R. 1981, ApJ, 246, 386
Wilhelm, K., Lemaire, P., Curdt, W., et al. 1997, Sol. Phys., 170, 75
Wilhelm, K. 2003, private communication
Witte, M., Rosenbauer, H., Banaszkiewicz, M., & Fahr, H. 1993, Adv. Space Res., 13(6), 121
Witte, M., Banaszkiewicz, M., & Rosenbauer, H. 1996, Space Sci. Rev., 78, 289
Witte, M. 2004, A&A, 426, 835
Witte, M., et al. 2004, Adv. Space Res., in press
Wolff, B., Koester, D., & Lallement, R. 1999, A&A, 346, 969